Published in *ASCE Journal of Geotechnical and Geoenvironmental Engineering*, 142(8), August http://dx.doi.org/10.1061/(ASCE)GT.1943-5606.0001498

A FAILURE ENVELOPE APPROACH FOR CONSOLIDATED UNDRAINED CAPACITY OF SHALLOW FOUNDATIONS

Cristina VULPE (corresponding author)
Centre for Offshore Foundation Systems & ARC Centre of Excellence
M053 University of Western Australia
35 Stirling Highway, Crawley, Perth, WA 6009, Australia
Tel: +61 8 6488 7051, Fax: +61 8 6488 1044
Email: cristina.vulpe@uwa.edu.au

Susan GOURVENEC
Centre for Offshore Foundation Systems & ARC Centre of Excellence
M053 University of Western Australia
35 Stirling Highway, Crawley, Perth, WA 6009, Australia
Tel: +61 8 6488 3995, Fax: +61 8 6488 1044
Email: susan.gourvenec@uwa.edu.au

Billy LEMAN (formerly a student at The University of Western Australia)
Wellbore Intervention Engineer
Baker Hughes Incorporated
256 St Georges Terrace, Perth, WA 6000, Australia
Tel: +61 8 9455 0174
Cell: +61 406 773 974
Email: billy.leman@bakerhughes.com

Kah Ngii FUNG (formerly a student at The University of Western Australia)
Design Assistant
CIMC Modular Building Systems (Australia) Pty Ltd
Level 10, 553 Hay Street, Perth, 6000 WA
Tel: +61 8 6214 3803

Published in *ASCE Journal of Geotechnical and Geoenvironmental Engineering*, 142(8), August http://dx.doi.org/10.1061/(ASCE)GT.1943-5606.0001498

Email: beverly.fung@cimc-mbs.com.au

No. of words: 4921 (exc. Abstract and References)

No. of tables: 4

No. of figures: 20

Published in *ASCE Journal of Geotechnical and Geoenvironmental Engineering*, 142(8), August http://dx.doi.org/10.1061/(ASCE)GT.1943-5606.0001498

Abstract:

A generalized framework is applied to predict consolidated undrained VHM failure envelopes for surface circular and strip foundations. The failure envelopes for consolidated undrained conditions are shown to be scaled from those for unconsolidated undrained conditions by the uniaxial consolidated undrained capacities, which are predicted through a theoretical framework based on fundamental critical state soil mechanics. The framework is applied to results from small strain finite element analyses for a strip and circular foundation of selected foundation dimension and soil conditions and the versatility of the framework is validated through a parametric study. The generalised theoretical framework enables consolidated undrained VHM failure envelopes to be determined for a practical range of foundation size and linearly increasing soil shear strength profile, through the expressions presented in this paper.

Key words: consolidation, bearing capacity, combined loading, failure envelope

Published in *ASCE Journal of Geotechnical and Geoenvironmental Engineering*, 142(8), August http://dx.doi.org/10.1061/(ASCE)GT.1943-5606.0001498

Introduction

Shallow foundations are often subjected to combined vertical, horizontal and moment (VHM) loading, particularly in a marine environment, derived from environmental or operational loading. Significant research has been carried out on the undrained capacity of shallow foundations under combined VHM loading (e.g. Martin & Houlsby 2001, Bransby & Randolph 1998, Ukritchon et al. 1998, Taiebat & Carter 2000, Gourvenec & Randolph 2003, Gourvenec 2007a, b, Bransby & Yun 2009, Gourvenec & Barnett 2011, Vulpe et al. 2013, Vulpe et al. 2014, Feng et al. 2014). Limited insight has been offered into the consolidated undrained response of shallow foundation systems, and most studies have investigated the consolidation effect on undrained vertical bearing capacity only (e.g. Zdravkovic et al. 2003, Lehane & Jardine 2003, Lehane & Gaudin 2005, Chatterjee et al. 2012, Gourvenec et al. 2014, Vulpe & Gourvenec 2014, Fu et al. 2015) and seldom combined capacity (Bransby 2002).

Undrained geotechnical resistance of a shallow foundation under any load path is dependent on the undrained shear strength of the supporting soil and can be increased by improvement of the undrained soil strength in the vicinity of a foundation. Consolidation due to preloading (including the self-weight of the foundation and the structure that it supports) causes the undrained shear strength of supporting soils to increase non-uniformly with depth and lateral extent, consistent with the pressure bulb developed from the applied foundation load. The soil immediately below the foundation experiences the largest change in shear strength, diminishing to the in situ strength in the far field. The degree of enhanced geotechnical resistance of a foundation is governed by the degree of overlap between the zone of undrained soil strength

improvement and the zone of soil involved in the kinematic mechanism accompanying subsequent failure.

In the case of pure horizontal loading, failure occurs in the uppermost soil layer coinciding with the zone of maximum shear strength increase – and considerable gain in sliding resistance would therefore be expected. In the case of pure vertical loading, the classical Prandtl or Hill failure mechanisms will extend laterally beyond the zone of enhanced soil strength and therefore less relative increase in vertical bearing capacity would be expected. A spectrum of kinematic mechanisms accompany failure under combined VHM loading with maximum relative gains to be achieved in cases of greatest overlap between the zone of maximum shear strength increase and the governing failure mechanism. Since many structures are affected by multi-directional loading, of duration to invoke an undrained soil response, the consolidated undrained response under three-dimensional loading of shallow foundations is of considerable practical interest. Particular applications include 1) reassessing the capacity of existing foundations to withstand future or additional moment and horizontal loading, 2) studying a foundation failure via back-calculation, and 3) reliance on consolidated undrained strength for geotechnical shallow foundation design, for example for subsea structures for which the foundation is set down, and the surrounding soil consolidates under the foundation and structure self-weight for a period of time (often several months or a year) in advance of operation at which stage multi-directional loading is applied.

The study presented in this paper systematically investigated the effects of the relative magnitude and duration of vertical preload on the undrained uniaxial vertical (V),

horizontal (H) and moment (M) capacity and combined VHM capacity of circular and strip surface foundations through finite element analyses (FEA).

Consolidated undrained capacities, V_{cu}, H_{cu} and M_{cu}, calculated in the FEA are predicted through a recently developed generalised critical state framework for shallow foundations (Gourvenec et al., 2014) while the normalised VHM interaction is shown to scale with relative preload and degree of consolidation through the consolidated undrained capacities.

The actual relative gains calculated by the FEA are particular to the foundation and soil conditions considered – but the theoretical framework, with the stress and strength factors provided in this paper, can be applied to a range of foundation dimensions and soil properties (and therefore undrained shear strength profiles). The encapsulating critical state framework extends the outcome of the results beyond the particular foundation dimension and soil conditions considered in the FEA to a generalised solution.

The value of this study lies in the demonstration that:

(i) consolidated undrained uniaxial capacities, V_{cu}, H_{cu} and M_{cu} can be predicted by the generalized critical state framework presented; and

(ii) consolidated undrained VHM failure envelopes scale from the unconsolidated undrained VHM failure envelope according to the consolidated uniaxial capacities (which can be predicted through the theoretical framework outlined in (i)).

Published in *ASCE Journal of Geotechnical and Geoenvironmental Engineering*, 142(8), August http://dx.doi.org/10.1061/(ASCE)GT.1943-5606.0001498

Finite element model

The study is based on small strain finite element analyses carried out with the commercial code Abaqus (Dassault Systèmes 2012).

Foundation geometry

Rigid circular and strip surface foundations with unit diameter (D) or breadth (B) were analysed in the FEA, i.e. D = B was nominally taken as 1 m. The particular foundation size selected for the FEA presented in the paper is arbitrary. A unit width foundation was selected for illustration of the theoretical framework, which can be applied to any foundation dimension through the dimensionless groups that the results are presented in. This generality is demonstrated in the Results section.

Soil conditions and material parameters

Normally consolidated (NC) clay with linearly increasing shear strength with depth was considered. Cam Clay parameters used in this study are based on element testing on kaolin clay (Stewart 1992, Chen 2005) and are summarized in Table 1. The soil behaviour is defined by a poro-elastic constitutive relationship pre-yield and by the Modified Cam Clay critical state constitutive model post-yield. The specific gravity of the soil is assumed constant and equal to 2.6, giving the buoyant unit weight as a function of initial void ratio e_0.

The coefficient of earth pressure at rest, after normal consolidation, is defined by

$$K_0 = 1 - \sin\phi_{cs} \qquad \textbf{1}$$

where ϕ_{cs} is the critical state internal friction angle. The in situ effective stresses vary accordingly to the prescribed soil unit weight (Table 1). The initial size of the yield envelope is prescribed as a function of the initial stresses in the soil

$$p_c' = \frac{q_0^2}{M_{cs}^2 p_0'} + p_0' \qquad \textbf{2}$$

where p_0' and q_0' are the in situ mean effective stress and deviatoric stress, respectively. M_{cs} represents the slope of the critical state line and takes the form:

$$M_{cs} = \frac{6\sin\phi_{cs}}{3-\sin\phi_{cs}} \qquad \textbf{3}$$

The in situ density of the soil is taken into account through the initial void ratio, e_0:

$$e_0 = e_1 - \kappa \ln p_0' - (\lambda - \kappa)\ln p_c' \qquad \textbf{4}$$

with

$$e_1 = e_{cs} + (\lambda - \kappa)\ln(2) \qquad \textbf{5}$$

The equivalent undrained shear strength of the normally consolidated clay layer is calculated from the critical state parameters using the expression given by Potts & Zdravkovic (1999):

$$\frac{s_u}{\sigma_v'} = g(\theta)\cos(\theta)\frac{1+2K_0}{3}\left(\frac{1+A^2}{2}\right)^{1-\frac{\kappa}{\lambda}} \qquad \textbf{6}$$

where θ = -30° is the Lode angle for triaxial conditions to ensure equilibrium of the K_0 consolidated initial stress state; σ'_v is the in situ effective vertical stress; and

$$g(\theta) = \frac{\sin(\phi_{cs})}{\cos\theta + \frac{1}{\sqrt{3}}\sin\theta\sin\phi_{cs}} \quad \textbf{7}$$

$$A = \frac{\sqrt{3}(1-K_0)}{g(-30^\circ)(1+2K_0)} \quad \textbf{8}$$

For the initial set of analyses, an overburden pressure σ'_{vo} equivalent to 1 m depth of soil was imposed across the free surface to define a non-zero shear strength at the mudline in the MCC model. The resulting undrained shear strength profile is linear with depth of the form

$$s_u = s_{um} + k_{su}z \quad \textbf{9}$$

where s_u represents the undrained shear strength at depth z, s_{um} is the mudline strength and k_{su} is the strength gradient. For the soil properties given in Table 1 and considered in the initial set of FEA, s_{um} = 4.79 kPa and k_{su} = 1.75 kPa/m.

The magnitude of the initial overburden pressure, and hence mudline strength, affects the magnitude of unconsolidated undrained capacity and relative gain in consolidated undrained capacity. However, the generalised framework presented to predict the consolidated capacity gains incorporates the effect of initial overburden, such that the methodology presented is applicable to a practical range of overburden (and foundation breadth or diameter). This is demonstrated in the Results section.

Finite element mesh

Three dimensional (3D) and plane strain finite element meshes were used to model the circular and strip foundation conditions respectively. Due to symmetry along the vertical centreline of the circular foundation, only half of the problem was modelled. A schematic representation of the plane strain finite element model is illustrated in Figure 1 and an example mesh is shown in Figure 2. The circular foundation model was constructed with boundary conditions and mesh discretisation in-plane identical to the plane strain model. The mesh boundaries extend 10 times the foundation diameter or breadth both horizontally and vertically from the centreline of the foundation in order to ensure the foundation response is unaffected by the boundary. Horizontal displacement was constrained on the vertical mesh boundaries and horizontal and vertical displacements were constrained across the base of the mesh. The free surface of the mesh, unoccupied by the foundation, was prescribed as a drainage boundary; the other mesh boundaries and the foundation were modelled as impermeable.

The circular and strip foundations were represented as rigid bodies with a single reference point (RP) located at the foundation centreline along the foundation-soil interface. The foundation-soil interface was defined as fully bonded, i.e., rough in shear and no separation permitted to represent that of shallowly skirted foundations, commonly used offshore. In reality, a skirted foundation comprises a top plate equipped with a peripheral skirt that penetrates into the seabed confining a soil plug. Negative excess pore pressures generated between the underside of the top plate and the soil plug enable tensile resistance (relative to ambient pressure) to be mobilised. It is common practice to model skirted foundations as a surface foundation with a fully bonded

foundation-soil interface (e.g. Tani & Craig 1995, Ukritchon et al. 1998, Bransby & Randolph 1998, Gourvenec & Randolph 2003, Yun & Bransby 2007). The plane strain and 3D finite element models were created with similar mesh discretisation in-plane with an optimum number of elements of 6,500 for the plane strain model and 20,000 for the 3D model.

Scope and loading methods

Initially, the unconsolidated undrained uniaxial vertical capacity, denoted V_{uu}, was determined for each foundation geometry through a displacement-controlled uniaxial vertical load path to failure. These analyses were carried out with the soil modelled as both a Modified Cam Clay (MCC) material and Tresca material to ensure consistency of results between constitutive models and with existing data. A series of MCC analyses was then carried out to determine the consolidated undrained capacity. In each analysis, the foundation was preloaded by a fraction of the unconsolidated undrained uniaxial vertical capacity, denoted V_p/V_{uu} (each foundation geometry was preloaded relative to the relevant undrained uniaxial vertical capacity, V_{uu}, and V_p was additional to the overburden pressure acting). The soil was then permitted to consolidate under the prescribed vertical preload before bringing the soil to undrained failure.

Relative preload, V_p/V_{uu}, was applied at intervals of 0.1 from 0.1 to 0.7 and partial or full primary consolidation was permitted prior to undrained failure. Periods corresponding 20, 50 and 80% of full primary consolidation, denoted T_{20}, T_{50} and T_{80}, respectively, were considered.

Following vertical preloading and consolidation for T_{20}, T_{50}, T_{80} and T_{99}, the soil was brought to undrained failure by means of displacement-controlled tests to determine the uniaxial consolidated undrained capacities, denoted V_{cu}, H_{cu} and M_{cu}, or by constant-ratio displacement probes to obtain the consolidated undrained capacities in VHM space. Pure uniaxial consolidated undrained capacity in each direction was obtained in the absence of other loadings other than the applied preload (e.g. V_{cu} for H = 0 and M = 0, but H_{cu} for $V = V_p$ and M = 0). Consolidated undrained failure envelopes were determined by first applying the preload level as a direct force on the foundation, and after consolidation, applying a constant-ratio displacement probe, $u/D\theta$, to failure (where u represents the horizontal translation and θ represents the rotation applied to the foundation reference point).

Sign convention and nomenclature

The sign convention for loads and displacements follows a right-handed axes and clockwise rotations rule, as proposed by Butterfield et al. (1997). The notations adopted for unconsolidated undrained and consolidated undrained capacities are summarized in Table 2.

Results

Validation

Unconsolidated undrained ultimate limit states were defined with both the Tresca and Modified Cam Clay constitutive models using the commercial finite element software, Abaqus. For the Tresca analyses, the Menetrey-Willam deviatoric ellipse function is used with the out-of-roundedness parameter, e, set to 1, giving a Von Mises circular

flow potential surface in the deviatoric plane while the yield surface remains the regular Tresca hexagon. For the MCC analyses, a Von Mises circular yield surface is used, by setting the flow stress ratio, K = 1.

The finite element models were validated against theoretical solutions where available. The undrained (unconsolidated) uniaxial vertical capacity predicted by the finite element models using the Tresca criterion was validated against lower bound solutions (Martin 2003) and agreed to within 2% for both the circular and strip foundation geometries. The undrained unconsolidated horizontal capacity of the surface foundations was compared with the theoretical solution (H_{uu}/As_{u0} = 1) and the undrained unconsolidated moment capacity was compared with theoretical upper bound solutions (Murff & Hamilton 1993, Randolph & Puzrin 2003). Both horizontal and moment capacities of the strip foundations agreed with the theoretical solutions to within 6% difference while the results diverged by 10% for the circular foundation due to poor representation of a spherical scoop failure mechanism with hexahedral elements. A mesh refinement study was undertaken to determine the optimum mesh discretisation for both foundation types by gradually increasing the number of elements around the foundation where the failure mechanism developed until further refinement did not improve the result.

The dissipation response calculated in the FEA cannot be directly validated against the classical elastic solution of time-settlement response (Booker & Small 1986) as the coefficient of consolidation, c_v, changes during the analysis with the elasto-plastic critical state model, in contrast to the constant c_v conditions of the elastic analysis. The consolidation response from the tests is discussed in more detail below.

Published in *ASCE Journal of Geotechnical and Geoenvironmental Engineering*, 142(8), August http://dx.doi.org/10.1061/(ASCE)GT.1943-5606.0001498

Consolidation response

The dissipation response under preloading of the foundations is illustrated in Figures 4 and 5 as time histories of consolidation settlement, w_c, normalised by foundation dimension (diameter D or breadth B) and by the final consolidation settlement, w_{cf}, measured at the centreline of the foundation along the foundation-soil interface. The immediate settlement following preloading is deducted from the total settlement to give the consolidation settlement, w_c. Time is expressed by the dimensionless factor

$$T = \frac{c_{v0}t}{D^2}\,;\; T = \frac{c_{v0}t}{B^2} \qquad \textbf{10}$$

where t represents the consolidation time, D or B is the foundation diameter or breadth and c_{v0} is the initial coefficient of consolidation:

$$c_{v0} = \frac{k(1+e_0)p_0^{'}}{\lambda\gamma_w} \qquad \textbf{11}$$

where k is the permeability of the soil, λ is the slope of normal compression line and γ_w = 9.81 kN/m^3 is the unit weight of water.

Figure 4 shows that consolidation settlement increases with increasing relative preload and is greater for the strip foundation compared with the circular foundation. Smaller settlements (half the magnitude) were obtained under the same level of relative preload in the same soil conditions for the circular foundation compared to the strip foundation due to lateral load shedding under three-dimensional conditions. Figure 5 shows that axisymmetric flow and strain around the circular foundation leads in general to a

reduction in dissipation time of around one order of magnitude compared with plane strain conditions.

The normalised time-settlement relationship for the circular foundation from the finite element analyses, modelled with critical state coupled consolidation constitutive model, agrees well with the classical elastic solution (Booker & Small 1986) initially, but as consolidation progresses, the elasto-plastic soil consolidates at a faster rate owing to the increasing stiffness of the soil as effective stresses increase. No elastic consolidation solution is available for a strip foundation.

Effect of full primary consolidation on uniaxial V, H and M capacity

Figure 6 shows the gain in uniaxial capacity as the ratio of the consolidated undrained capacity to the unconsolidated undrained capacity for vertical ($v_{cu} = V_{cu}/V_{uu}$), horizontal ($h_{cu} = H_{cu}/H_{uu}$) and moment ($m_{cu} = M_{cu}/M_{uu}$) loading. Results are shown for the circular and strip foundations after vertical preloading and full primary consolidation. The term uniaxial is usually reserved for loading in one direction with zero loading in any other direction, e.g. uniaxial H loading in the absence of vertical load or moment. In this paper, the term uniaxial is taken to define loading in only one direction over and above the vertical preload, e.g. uniaxial H loading in the presence of the vertical preload but no additional vertical load or moment.

The relative gain in capacity increases with the level of vertical preload under each load path and potentially significant gains are achieved in each case. The highest relative gain in capacity is observed under horizontal loading (following vertical preload and consolidation). The lowest relative gain is observed under vertical loading (following

vertical preload and consolidation). Shape effects were not observed in the relative gain in capacity under vertical and horizontal loading, while a greater relative gain in moment capacity was observed for the strip foundation than the circular foundation. The observed trends in relative gain in capacity can be explained by considering the interaction between the zone of shear strength increase and the kinematic mechanisms accompanying failure.

Figure 7 compares the increase in shear strength due to full primary consolidation beneath circular and strip foundations for levels of relative preload V_p/V_{uu} = 0.1, 0.4 and 0.7. The change in undrained shear strength is illustrated through contours of enhanced soil strength relative to the in situ value, $s_{u,f}/s_{u,i}$ defined as

$$\frac{s_{u,f}}{s_{u,i}} = \exp\left(\frac{e_0 - e_f}{\lambda}\right) \qquad \textbf{12}$$

where $s_{u,i}$ and $s_{u,f}$ are the in situ and final (i.e. post-consolidation) shear strength, e_0 and e_f are the in situ and final void ratio and λ is the virgin compression index for kaolin clay (Stewart 1992).

The extent of the zone of enhanced shear strength increases with level of relative preload and is more extensive beneath the strip foundation than the circular foundation due to the confinement of load shedding in-plane under plane strain conditions.

The relative gain in capacity of a foundation following a period of consolidation is governed by the overlap between the zone of shear strength increase and failure mechanism. Figure 8 shows contours of shear strength increase in the soil mass beneath

the circular foundation under a preload V_p/V_{uu} = 0.4, overlaid by velocity vectors at failure under uniaxial vertical load, horizontal load and moment. It is clear that the horizontal failure mechanism is almost entirely confined in the zone of maximum strength increase, close to the foundation-soil interface, and is associated with the greatest relative gain in capacity. The moment failure mechanism is confined within the zone of strength increase, but penetrates into the soil mass into zones of lesser strength enhancement, which is reflected in a lower relative gain in capacity. The vertical failure mechanism is seen to extend into the soil mass, benefitting least from the consolidation process, and also laterally beyond the region of shear strength increase, and is associated with the lowest relative gain in capacity.

The reason for the similar observed relative gain in capacity under vertical loading for both strip and circular foundations is illustrated in Figure 9. The failure mechanisms for both strip and circular foundations cut through zones of soil of equal increase in shear strength. Although the size of the failure mechanisms varies with foundation shape, the size of the zone of enhanced strength varies similarly. The greater observed relative gain in moment capacity for the strip foundation compared with the circular foundation is explained by Figure 10 that compares the zone of shear strength increase and extent of the failure mechanisms in the two cases. The failure mechanism for the strip foundation occurs in soil with higher shear strength increase while the circular foundation failure mechanism reaches into soil with lesser strength enhancement. In this case, the extent of the zone of sheared soil is similar for both foundation shapes but the zone of increased shear strength is dependent on foundation geometry.

Critical state framework

The relative gain in undrained capacity following consolidation is interpreted through fundamental critical state soil mechanics (CSSM) (Schofield & Wroth 1968). A CSSM framework for predicting gain in undrained vertical capacity of surface strip and circular foundations for a range of over consolidation ratios was set out by Gourvenec et al. (2014). That method is applied and extended here to predict gains in undrained uniaxial but multi-directional capacity of surface strip and circular foundations.

The mobilised soil below the pre-loaded foundation is considered as a single 'operative' element, which for initially normally consolidated conditions, the increment in operative stress due to the preload can be estimated as

$$\Delta\sigma'_{pl} = f_\sigma v_p = f_\sigma \frac{V_p}{A} \qquad \textbf{13}$$

where v_p is the preload stress given by the applied vertical preload V_p divided by the area of the foundation A, and the stress factor f_σ accounts for the non-uniform distribution of the stress in the affected zone of soil. Gourvenec et al. (2014) present more general expressions for over-consolidated conditions.

The resulting increase in the operative strength of the soil involved in the subsequent failure mechanism is then calculated as

$$\Delta s_u = f_{su} R\left(\Delta\sigma'_{pl}\right) = f_\sigma f_{su} R\left(\frac{V_p}{A}\right) \qquad \textbf{14}$$

where the shear strength factor f_{su} scales the gain in strength from that caused by $\Delta\sigma'_{pl}$ to that mobilised throughout the subsequent failure, and R is the normally-consolidated strength ratio of the soil, s_u/σ'_v = 0.279 for the MCC parameters given in Table 1.

Separate scaling factors, f_σ and f_{su}, allow the response in over-consolidated conditions to be captured (Gourvenec et al. 2014), but in the present normally-consolidated conditions there is effectively a single scaling parameter, $f_\sigma f_{su}$.

Capacity is then assumed to scale with the change in operative strength, so that

$$\frac{V_{cu}}{V_{uu}}, \frac{H_{cu}}{H_{uu}}, \frac{M_{cu}}{M_{uu}} = 1 + \frac{\Delta s_u}{s_u} = 1 + f_\sigma f_{su} R\left(\frac{V_p}{V_{uu}}\right) N_{cV} \qquad \textbf{15}$$

where N_{cV} is the unconsolidated undrained vertical bearing capacity factor defined as V_{uu}/As_{u0} and the factor $f_\sigma f_{su}$ is fitted to give the best agreement with the observed gains from the FEA for each load path direction. Derived factors $f_\sigma f_{su}$ for uniaxial vertical, horizontal and moment capacity for strip and circular foundation geometry are summarised in Table 3.

Extension to partially consolidated undrained uniaxial capacity

Determining the gain in capacity over time, not solely after full dissipation of excess pore water pressure, is of practical interest since often sufficient time is not available to achieve full primary consolidation. Figure 11 illustrates the evolution of the proportion of maximum potential gain in undrained vertical and horizontal capacity as a function of consolidation time. A simple equation linking the consolidation time, represented by the non-dimensional time factor T, and the proportion of maximum potential gain (i.e. following full primary consolidation) is proposed:

$$\frac{V_{cu,p}-V_{uu}}{V_{cu}-V_{uu}},\frac{H_{cu,p}-H_{uu}}{H_{cu}-H_{uu}},\frac{M_{cu,p}-M_{uu}}{M_{cu}-M_{uu}}=\frac{1}{1+m\left(\frac{T}{T_{50}}\right)^{n}} \qquad \textbf{16}$$

from which the partial relative gains in undrained uniaxial capacity, $V_{cu,p}$, $H_{cu,p}$ and $M_{cu,p}$ may be determined. The non-dimensional time factor for 50% consolidation T_{50} is 0.21 and 1.50 for circular and strip foundations, respectively. Fitting coefficients n = -1.20 and m are given in Table 4 for each loading direction. Figure 11 indicates good agreement between the FEA results for a variety of discrete levels of preload, V_p/V_{uu}, and the relative gains in undrained uniaxial capacity derived from Equation (16).

Parametric study for scale effects and soil properties

To demonstrate the generality of the theoretical method outlined above, a parametric study varying the foundation size and soil properties was conducted.

Figure 12 compares finite element analyses results and predictions from the theoretical method for circular foundations with diameter D = 1 m and 10 m for constant $\kappa_{su} = k_{su}D/s_{um}$ modelled with the MCC parameters given in Table 1. The critical state framework shows that the relative gain in capacity in all uniaxial directions is independent of the actual foundation size provided the dimensionless group $\kappa_{su} = k_{su}D/s_{um}$ is constant. The relative gain in capacity is governed only by the stress and strength factor $f_\sigma f_{su}$, normally consolidated in situ strength ratio R and undrained vertical bearing capacity factor N_{cV}. Given that the soil conditions and dimensionless soil strength heterogeneity are identical in both cases, R and N_{cV} are constant, Figure 12

shows that the derived $f_\sigma f_{su}$ factor captures the change in gain in strength irrespective of foundation size.

Figure 13 demonstrates the applicability of the critical state framework with unique $f_\sigma f_{su}$ values to capture relative gains in foundation capacity for a range of MCC input parameters. FEA were carried out where critical state parameter values κ/λ and M_{cs} were altered, while keeping all other parameters from Table 1 identical. Although the value of R changes for varying κ/λ and M_{cs}, the critical state framework accurately captures the changing gains in capacity using the same $f_\sigma f_{su}$ values from Table 3.

Figure 14 demonstrates the applicability of the critical state framework with unique $f_\sigma f_{su}$ values to capture the relative gains in foundation capacity for different values of overburden stress σ'_{vo} to define the initial stress state and mudline strength intercept. The theoretical framework has been shown to accurately predict gains for a practical range of overburden (which is expressed dimensionlessly via the variation in $\kappa_{su} = k_{su}D/s_{um}$) with unique values of $f_\sigma f_{su}$ for a given foundation geometry and load path.

The cases shown in Figure 14 capture the practical range of κ_{su} for which surface foundations are used. For higher κ_{su} the low mudline strength means that foundation skirts are required in order to achieve a practical bearing capacity. The critical state framework is equally applicable to foundations with shallow skirts, as demonstrated by the additional results and prediction line shown in Figure 14a. These results are from independent FEA of consolidated bearing capacity reported by Fu et al. (2015), using similar soil parameters to the present study and a circular foundation with skirts to a

depth of 20% of the diameter. The theoretical framework yields predictions that lie within 3% of the Fu et al. (2015) numerical results.

Effect of consolidation on combined capacity

Failure envelopes in horizontal and moment load space for discrete levels of relative vertical preload (V_p/V_{uu} = [0.1, 0.7]) followed by full primary consolidation are compared with the unconsolidated undrained case in Figure 15. The failure envelopes are presented in terms of loads normalised by the respective unconsolidated undrained capacity, H_{uu} and M_{uu}, i.e. $h = H/H_{uu}$ vs. $m = M/M_{uu}$.

The effect of increasing vertical load without consolidation results in contraction of the failure envelope (as seen in Figure 15 a and b), indicating a reduction in capacity. In contrast, increasing vertical load coupled with consolidation leads to expansion of the failure envelope (Figure 15c and d), indicating increasing capacity.

The results also show that the shape of the normalised H-M failure envelope for a given vertical load is similar for the consolidated and unconsolidated cases, as shown in Figure 16 for discrete levels of preload V_p/V_{uu} = 0.3 and 0.6. This observation enables consolidated undrained failure envelopes to be constructed by simple scaling of the unconsolidated undrained failure envelope by the consolidated undrained uniaxial horizontal and moment capacity, H_{cu} and M_{cu} (following partial or full primary consolidation).

The similitude of the failure envelopes for consolidated undrained conditions to those for unconsolidated undrained conditions is reflected in the similitude of failure

mechanisms under combined loads with and without consolidation as illustrated in Figure 17 for a selected H/M load path.

Approximating expressions for VHM envelopes

Undrained (unconsolidated) capacity

An approximating expression based on a rotated ellipse is suitable for predicting the unconsolidated undrained failure envelopes of shallow foundations:

$$\left(\left|\frac{h}{h^*}\right|\right)^{\alpha} + \left(\frac{m}{m^*}\right)^{\beta} + 2\mu\frac{hm}{h^* m^*} - 1 = 0 \qquad \textbf{17}$$

where $h = H/H_{uu}$ and $m = M/M_{uu}$ define the normalised unconsolidated undrained horizontal load and moment mobilisation.

The form of the expression was originally proposed for prediction of (unconsolidated) undrained capacity of shallow strip and circular foundations under general loading (Gourvenec & Barnett 2011). An additional fitting parameter, μ, which controls the eccentricity of the ellipse, has been incorporated into the original expression to improve the fit.

h^* and m^* represent the normalized unconsolidated horizontal and moment capacities as a function of relative vertical preload V_p/V_{uu} for which conservative approximating expressions have been previously derived (Gourvenec & Barnett 2011, Vulpe et al. 2014):

$$h^* = 1 - \left(\frac{V_p}{V_{uu}}\right)^{4.69}$$

$$m^* = 1 - \left(\frac{V_p}{V_{uu}}\right)^{2.12} \quad \textbf{18}$$

for circular foundations and

$$h^* = 1 - \left(\frac{V_p}{V_{uu}}\right)^{3.59}$$

$$m^* = 1 - \left(\frac{V_p}{V_{uu}}\right)^{3.41} \quad \textbf{19}$$

for strip foundations.

Gourvenec & Barnett (2011) proposed polynomials for fitting the vh (m = 0) and vm (h = 0) interactions, i.e. h* and m* here, of strip foundations. The original data has been refitted with a power law for a better fit and for consistency with the expressions adopted for the circular foundation geometry.

Fitting parameters α, β and μ capture the change in size and shape of the unconsolidated undrained failure envelopes as a function of relative preload V_p/V_{uu}. Unique fitting parameters α, β and μ for circular and strip foundations can be described by linear functions of relative preload:

$$\alpha = -2.20\frac{V_p}{V_{uu}} + 4.30 \quad \textbf{20}$$

Published in *ASCE Journal of Geotechnical and Geoenvironmental Engineering*, 142(8), August http://dx.doi.org/10.1061/(ASCE)GT.1943-5606.0001498

$$\beta = -0.62\frac{V_p}{V_{uu}} + 1.90 \qquad \textbf{21}$$

$$\mu = 0.48\frac{V_p}{V_{uu}} - 0.35 \qquad \textbf{22}$$

The unconsolidated undrained failure envelopes for circular and strip foundations, are shown as two-dimensional slices in the HM plane of three-dimensional VHM failure envelopes in dimensionless space $h/h^* - m/m^*$ in Figure 18 compared with the approximating expression. The curves resulting from the approximating expression show good agreement with the FEA results and capture the changing shape of the failure envelopes with varying level of preload.

Consolidated undrained capacity

As indicated in Figure 15 and Figure 16, an approximation of the consolidated undrained failure envelope can be achieved by scaling the normalised unconsolidated undrained VHM failure envelope (Eqn 17) by the corresponding consolidated undrained uniaxial horizontal and moment capacities, h_{cu} and m_{cu}, for each level of preload (from Eqn 15) and various consolidation times (from Eqn 16). Figure 19 and Figure 20 compare the FEA results against the approximating approach described here and show good agreement.

Example application

Taking a hypothetical but realistic example of a subsea structure supported by a 5 m diameter circular surface foundation, imposing a self-weight preload V_p/V_{uu} = 0.5 to a

typical deep offshore seabed with coefficient of consolidation, c_v = 10 m^2/yr, the results presented in this study show a maximum potential gain of 45 % in the undrained vertical capacity and 92 % in the undrained sliding capacity, i.e. for full primary consolidation (Figure 6). A half year time lag between foundation set down and operation would lead to 77 % of the maximum gain in vertical capacity and 84 % of the maximum gain in sliding capacity, i.e. an overall increase in undrained vertical capacity of $1.35V_{uu}$ and in horizontal sliding capacity of $1.78H_{uu}$. The same foundation under the same loading resting on a seabed with an order of magnitude greater coefficient of consolidation would achieve the same gains in an order of magnitude less time (~18 days). These time frames are realistic for offshore field operations and offer significant improvements in undrained capacity, which can be translated into smaller foundation footprints.

Concluding remarks

A generalised critical state framework in conjunction with the failure envelope approach has been applied to quantify the effect of vertical preloading and consolidation on the undrained VHM capacity of circular and strip surface foundations on normally consolidated clay. The outcomes of this study are summarized as follows:

- Three-dimensional flow and strain led to higher consolidation rates and smaller consolidation settlements of the circular foundation compared to the strip foundation under vertical preload.

- Greatest relative gain in capacity was observed under pure horizontal load, relative gain in moment capacity was intermediate and the lowest gain was associated with pure vertical capacity.

- Relative gains in capacity have been explained in terms of the overlap of zones of shear strength increase and the kinematic mechanism accompanying failure.

- The magnitude of relative gain under uniaxial vertical, horizontal and moment loading has been described within a generalised critical state framework that is applicable to a practical range of foundation dimensions and overburden pressures.

- Relative gains in uniaxial capacity under uniaxial vertical, horizontal and moment loading following partial consolidation have been estimated as a function of non-dimensional consolidation time and an approximating expression is presented.

- The full or partially-consolidated undrained VHM failure envelope for circular or strip foundations represents an expansion of the unconsolidated undrained VHM failure envelope at a given relative preload and degree of consolidation. The consolidated undrained VHM failure envelope can be determined by scaling the unconsolidated undrained envelope by the respective uniaxial consolidated undrained horizontal and moment capacities, which can be predicted by the critical state framework.

The study presented in this paper highlights the potential benefit of increases in the undrained soil strength from preloading and a period of consolidation when designing shallow foundations against multi-directional loading following. The generalised method provides a simple basis to estimate these potentially significant gains in capacity, which are most significant under load paths associated with near-surface kinematic mechanisms, such as those dominated by sliding.

Acknowledgements

This work forms part of the activities of the Centre for Offshore Foundation Systems (COFS). Established in 1997 under the Australian Research Council's Special Research Centres Program. Supported as a node of the Australian Research Council's Centre of Excellence for Geotechnical Science and Engineering, and through the Fugro Chair in Geotechnics, the Lloyd's Register Foundation Chair and Centre of Excellence in Offshore Foundations and the Shell EMI Chair in Offshore Engineering. The second author is supported through ARC grant CE110001009. The work presented in this paper is supported through ARC grant DP140100684. This support is gratefully acknowledged.

REFERENCES

Booker, J.R. and Small, J.C (1986). The behaviour of an impermeable flexible raft on a deep layer of consolidating soil. *International Journal for Numerical and Analytical Methods in Geomechanics*, 10: 311 – 327.

Bransby, M.F. (2002). The undrained inclined load capacity of shallow foundations after consolidation under vertical loads. *Proc. 8th Numerical Models in Geomechanics (NUMOG)*, Rome, 431-437.

Bransby, M.F. and Randolph, M.F. (1998). Combined loading of skirted foundations. *Géotechnique*, 48(5): 637-655.

Bransby, M.F. and Yun, G.J. (2009). The undrained capacity of skirted strip foundations under combined loading. *Géotechnique*, 59(2): 115-125.

Butterfield, R. and Banerjee, P.K. (1971). A rigid disc embedded in an elastic half space. *Geotechnical Engineering*, 2(1): 35-52.

Butterfield, R., Houlsby, G.T. and Gottardi, G. (1997). Standardised sign conventions and notation for generally loaded foundations. *Géotechnique*, 47(4): 1051–1052.

Chatterjee, S., Yan, Y., Randolph, M.F. and White, D.J. (2012). Elastoplastic consolidation beneath shallowly embedded offshore pipelines. *Géotechnique Letters* 2: 73-79.

Chen, W. (2005). *Uniaxial behaviour of suction caissons in soft deposits in deepwater*. PhD thesis, University of Western Australia.

Dassault Systèmes (2012). Abaqus analysis user's manual. Simulia Corp. Providence, RI, USA.

Davis, E.H. and Poulos, H.G. (1972). Rate of settlement under two- and three-dimensional conditions. *Géotechnique*, 22(1): 95 - 114.

Feng, X., Randolph, M. F., Gourvenec, S. and Wallerand, R. (2014) Design approach for rectangular mudmats under fully three dimensional loading, *Géotechnique* 64(1): 51-63.

Fu, D., Gaudin, C., Tian, C., Bienen, B. and Cassidy, M.J. (2015). Effects of preloading with consolidation on undrained bearing capacity of skirted circular footings. Géotechnique, 65(3): 231-246.

Gourvenec, S. (2007a). Failure envelopes for offshore shallow foundations under general loading. *Géotechnique*, 57(3): 715–728.

Gourvenec, S. (2007b) Shape effects on the capacity of rectangular footings under general loading. *Géotechnique*, 57(8): 637-646.

Gourvenec, S. and Barnett, S. (2011). Undrained failure envelope for skirted foundations under general loading. *Géotechnique*, 61(3): 263–270.

Gourvenec, S.M. and Mana, D.S.K. (2011). Undrained vertical bearing capacity factors for shallow foundations. Géotechnique Letters, 1(4): 101 – 108.

Gourvenec, S. and Randolph, M.F. (2003). Effect of strength non-homogeneity on the shape and failure envelopes for combined loading of strip and circular foundations on clay. *Géotechnique*, 53(6): 575-586.

Gourvenec, S. and Randolph, M.F. (2009). Effect of foundation embedment and soil properties on consolidation response, *Proc. Int. Conf. Soil Mechanics and Geotechnical Engineering (ICSMGE)*, Alexandria, Egypt. 638-641.

Gourvenec, S. and Randolph, M.F. (2010) Consolidation beneath skirted foundations due to sustained loading. *International Journal of Geomechanics*, 10(1): 22 - 29.

Gourvenec, S.M., Vulpe, C. and Murthy, T.G. (2014). A method for predicting the consolidated undrained bearing capacity of shallow foundations. *Géotechnique*, 64(3): 215 – 225.

Lehane, B.M. and Gaudin, C. (2005). Effects of drained pre-loading on the performance of shallow foundations on over consolidated clay. *Proc. Offshore Mechanics and Arctic Engineering* (OMAE), OMAE2005-67559.

Lehane, B.M. and Jardine, R.J. (2003). Effects of long-term preloading on the performance of a footing on clay. *Géotechnique*, 53(8): 689 - 695.

Martin, C.M. and Houlsby, G.T. (2001). Combined loading of spudcan foundations on clay: numerical modelling. *Géotechnique*, 51(8): 687–699.

Martin, C.M. (2003). New software for rigorous bearing capacity calculations. *Proc. British Geotech. Assoc. Int. Conf. on Foundations*, Dundee, 581-592.

Murff, J.D. and Hamilton, J.M. (1993). P-ultimate for undrained analysis of laterally loaded piles. *J. Geot. Eng. Div., ASCE* 119(1): 91-107.

Potts, D.M. and Zdravkovic, L. (1999). *Finite element analysis in geotechnical engineering – theory*. London, UK: Thomas Telford.

Randolph, M. F and Puzrin, A. M (2003). Upper bound limit analysis of circular foundations on clay under general loading. *Géotechnique*, 53(9): 785-796.

Schofield, A.N. and Wroth, C.P. (1968). *Critical state soil mechanics*. London, UK: McGraw-Hill.

Stewart, D.P. (1992). *Lateral loading of pile bridge abutments due to embankment construction*. PhD thesis, University of Western Australia.

Taiebat, H.A. and Carter, J.P. (2000). Numerical studies of the bearing capacity of shallow foundations on cohesive soil subjected to combined loading. *Géotechnique*, 50(4): 409–418.

Tani, K. and Craig, W.H. (1995). Bearing capacity of circular foundations on soft clay of strength increasing with depth. *Soils and Foundations*, 33(4): 21-35.

Ukritchon, B., Whittle, A.J. and Sloan, S.W. (1998). Undrained limit analysis for combined loading of strip footings on clay. *J. Geot. and Geoenv. Eng., ASCE* 124(3): 265-276.

Vulpe, C., Bienen, B. and Gaudin, C. (2013). Predicting the undrained capacity of skirted spudcans under combined loading. *Ocean Engineering*, 74: 178-188.

Vulpe, C. and Gourvenec, S. (2014). Effect of preloading on the response of a shallow skirted foundation. *Proceedings of the 33rd International Conference on Ocean, Offshore and Arctic Engineering (OMAE2014)*, San Francisco, USA, OMAE2014-23440.

Vulpe, C., Gourvenec, S. and Power, M. (2014). A generalised failure envelope for undrained capacity of circular shallow foundations under general loading. *Géotechnique Letters*, 4: 187 – 196 (http://dx.doi.org/10.1680/geolett.14.00010).

Wroth, C.P. (1984). The interpretation of in-situ soil tests. 24th Rankine Lecture, *Géotechnique*, 34(4): 449 - 489.

Yun, G. and Bransby, M.F. (2007). The undrained vertical bearing capacity of skirted foundations. Soils Foundations 47(3): 493-506.

Zdravkovic, L. Potts, D.M. and Jackson, C. (2003). Numerical study of the effect of preloading on undrained bearing capacity. *Int. J. Geomechanics* ASCE, September, 1 – 10.

Published in *ASCE Journal of Geotechnical and Geoenvironmental Engineering*, 142(8), August http://dx.doi.org/10.1061/(ASCE)GT.1943-5606.0001498

LIST OF TABLES

Table 1. Soil properties used in finite element analyses.

Table 2. Definition of notations for loads and displacements.

Table 3. Stress and strength factor $f_{\sigma}f_{su}$ for fully consolidated gain in uniaxial capacity for surface circular and strip foundations.

Table 4. Fitting coefficient m for determining the gain in capacity following partial consolidation for surface circular and strip foundations.

Published in *ASCE Journal of Geotechnical and Geoenvironmental Engineering*, 142(8), August http://dx.doi.org/10.1061/(ASCE)GT.1943-5606.0001498

TABLES

Parameter input for FEA	Magnitude
Index and engineering parameters	
Saturated Bulk Unit Weight (kN/m^3)	17.18
Specific gravity (G_s)	2.6
Permeability (m/s)	1.3 E-010
Elastic parameters (as a porous elastic material)	
Recompression Index (κ)	0.044
Poisson's Ratio (ν')	0.25
Tensile Limit	0
Clay plasticity parameters	
Virgin compression Index (λ)	0.205
Stress Ratio at Critical State (M_{cs})	0.89
Wet Yield Surface Size*	1
Flow Stress Ratio**	1
Intercept (e_1, at p'=1 on CSL)	2.14

*The wet yield surface size is a parameter defining the size of the yield surface on the "wet" side of critical state, β. (β = 1 means that the yield surface is a symmetric ellipse).
**The flow stress ratio represents the ratio of flow stress in triaxial tension to the flow stress in triaxial compression

Table 1. Soil properties used in finite element analyses.

Published in *ASCE Journal of Geotechnical and Geoenvironmental Engineering*, 142(8), August http://dx.doi.org/10.1061/(ASCE)GT.1943-5606.0001498

	Vertical	**Horizontal**	**Rotational**
Displacement	w	u	θ
Load	V_p (preload)	H	M
Uniaxial (unconsolidated) undrained capacity	V_{uu}	H_{uu}	M_{uu}
Unconsolidated undrained bearing capacity factor	$N_{cV} = V_{uu}/As_{u0}$	$N_{cH} = H_{uu}/As_{u0}$	$N_{cM} = M_{uu}/ADs_{u0}$
Normalized load	$v = V_p/V_{uu}$	$h = H/H_{uu}$	$m = M/M_{uu}$
Pure uniaxial consolidated undrained capacity	V_{cu}	H_{cu}	M_{cu}
Normalized pure uniaxial consolidated undrained capacity	$v_{cu} = V_{cu} / V_{uu}$	$h_{cu} = H_{cu} / H_{uu}$	$m_{cu} = M_{cu} / M_{uu}$

Table 2. Definition of notations for loads and displacements.

	$f_\sigma f_{su}$	
Loading direction	**circular**	**strip**
V	0.43	0.49
H	0.88	1.00
M	0.57	0.73

Table 3. Stress and strength factor $f_\sigma f_{su}$ for fully consolidated gain in uniaxial capacity for surface circular and strip foundations.

Loading direction	**m**
V	0.32
H	0.20
M	0.50

Table 4. Fitting coefficient m for determining the gain in capacity following partial consolidation for surface circular and strip foundations.

Published in *ASCE Journal of Geotechnical and Geoenvironmental Engineering*, 142(8), August http://dx.doi.org/10.1061/(ASCE)GT.1943-5606.0001498

LIST OF FIGURES

Figure 1. Schematic representation of the strip foundation model.

Figure 2. Example of finite element mesh for plane strain analysis.

Figure 3. Sign convention and notation nomenclature used in the study.

Figure 4. Non-dimensional time-settlement response for strip and circular foundations from FEA results.

Figure 5. Normalized time-settlement response of strip and circular foundations from FEA results compared to theoretical elastic solution with constant c_v.

Figure 6. Gain in uniaxial capacity for strip and circular foundations as a function of relative preload V_p/V_{uu}.

Figure 7. Contours of relative shear strength gain after full primary consolidation; circular and strip foundations.

Figure 8. Failure mechanisms under pure horizontal, moment and vertical loading following preloading and consolidation for the discrete level of preload V_p/V_{uu} = 0.4 (circular foundation) (Contour lines represent the relative change in shear strength).

Figure 9. Comparison of failure mechanisms of circular and strip foundations under pure vertical loading following preloading and consolidation for a discrete level of preload V_p/V_{uu} = 0.4 (Contour lines represent the relative change in shear strength).

Figure 10. Comparison of failure mechanisms of circular and strip foundations under pure moment loading following preloading and consolidation for a discrete level of preload V_p/V_{uu} = 0.4 (Contour lines represent the relative change in shear strength).

Figure 11. Gain in uniaxial capacity as a function of non-dimensional time factor T: comparison between FEA and Equation (16).

Figure 12. Sensitivity study showing applicability of theoretical framework to variations in foundation size of circular foundations for constant soil heterogeneity index κ_{su}.

Figure 13. Sensitivity study showing applicability of theoretical framework to varying MCC input for circular foundations

Figure 14. Sensitivity study showing applicability of theoretical framework to varying overburden for constant foundation size for circular foundations.

Figure 15. (a, b) Unconsolidated and (c, d) consolidated undrained failure envelopes as a function of relative preload for full primary consolidation (T_{99})

Figure 16. Comparison of shape of normalized failure envelopes for unconsolidated and fully consolidated undrained capacity of a circular foundation: a) $V_p/V_{uu} = 0.3$, b) $V_p/V_{uu} = 0.6$.

Figure 17. Failure mechanisms under undrained load paths to failure in HM space ($u/D\theta = 1$) for circular foundation.

Figure 18. Unconsolidated undrained normalized failure envelope for varying relative preload; FEA results and approximating expression (a) circular foundation and (b) strip foundation.

Figure 19. Consolidated undrained normalized failure envelope for varying relative preload after full primary consolidation; FEA results and approximating expression (a) circular foundation and (b) strip foundation.

Figure 20. Consolidated undrained normalized failure envelope for a discrete relative preload V_p/V_{uu} = 0.3 and varying consolidation times; FEA results and approximating expression (a) circular foundation and (b) strip foundation.

Published in *ASCE Journal of Geotechnical and Geoenvironmental Engineering*, 142(8), August http://dx.doi.org/10.1061/(ASCE)GT.1943-5606.0001498

FIGURES

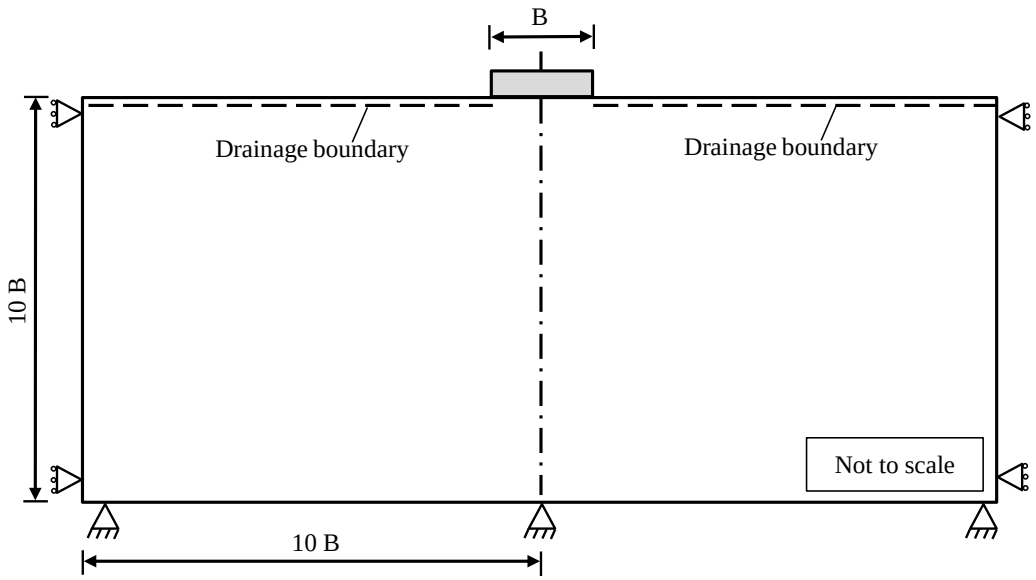

Figure 21. Schematic representation of the strip foundation model.

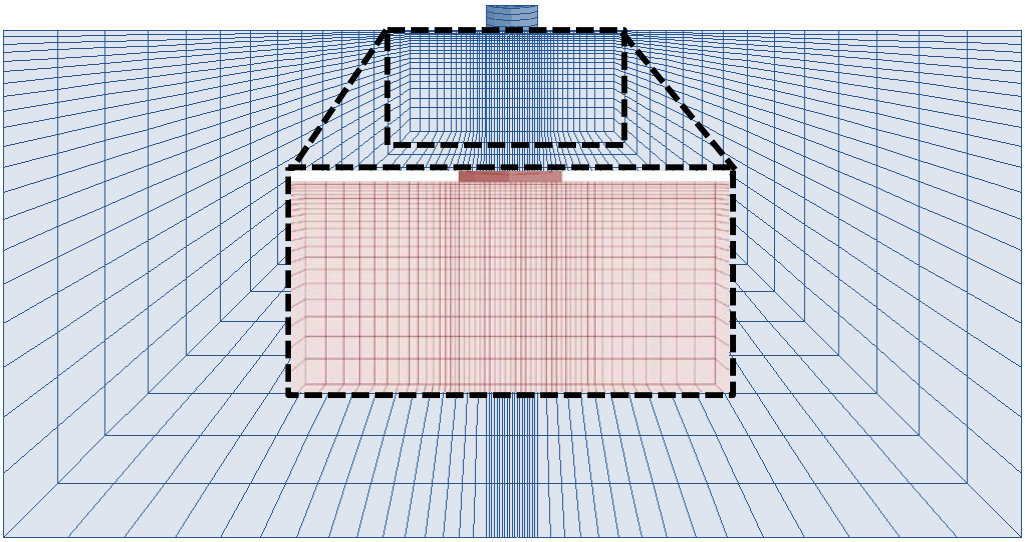

Figure 22. Example of finite element mesh for plane strain analysis.

Published in *ASCE Journal of Geotechnical and Geoenvironmental Engineering*, 142(8), August http://dx.doi.org/10.1061/(ASCE)GT.1943-5606.0001498

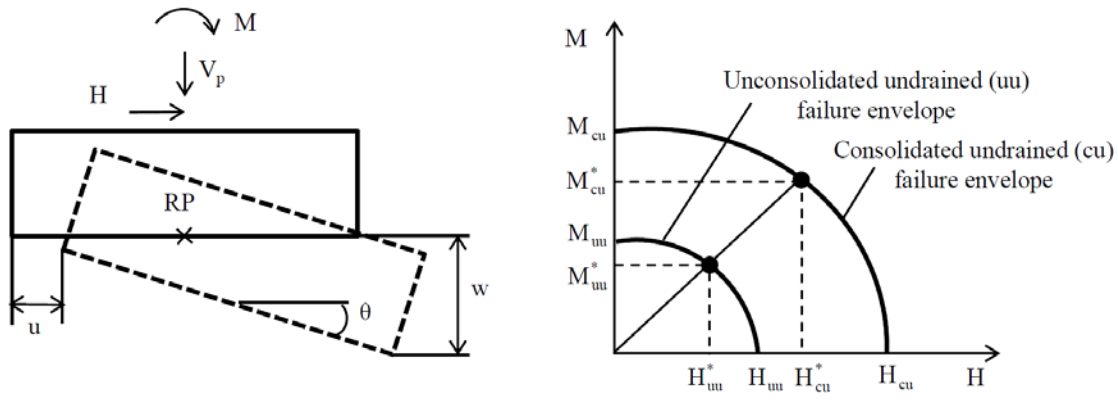

Figure 23. Sign convention and notation nomenclature used in the study.

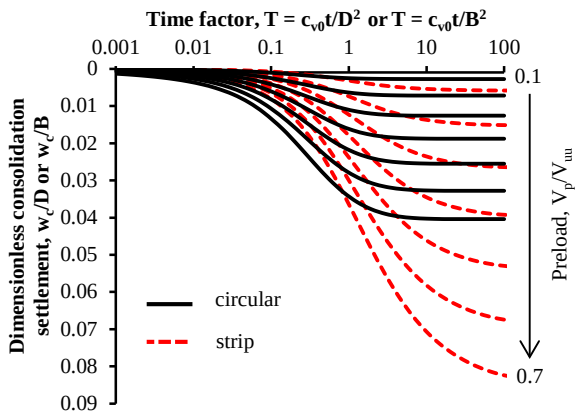

Figure 24. Non-dimensional time-settlement response for strip and circular foundations from FEA results.

Published in *ASCE Journal of Geotechnical and Geoenvironmental Engineering*, 142(8), August http://dx.doi.org/10.1061/(ASCE)GT.1943-5606.0001498

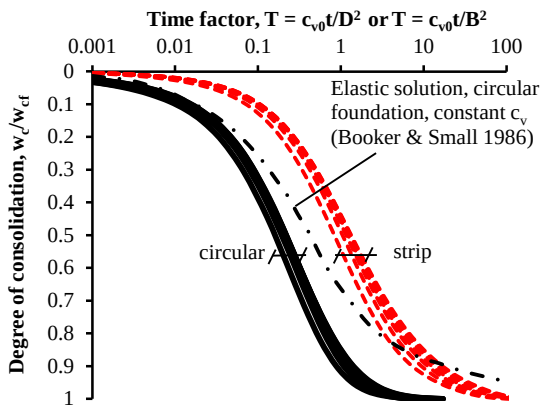

Figure 25. Normalized time-settlement response of strip and circular foundations from FEA results compared to theoretical elastic solution with constant c_v.

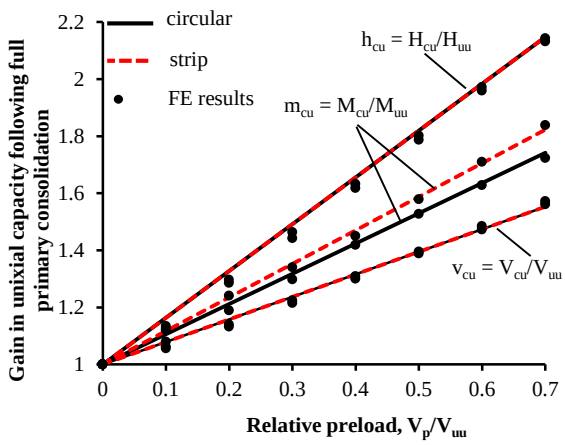

Figure 26. Gain in uniaxial capacity for strip and circular foundations as a function of relative preload V_p/V_{uu}.

Published in *ASCE Journal of Geotechnical and Geoenvironmental Engineering*, 142(8), August http://dx.doi.org/10.1061/(ASCE)GT.1943-5606.0001498

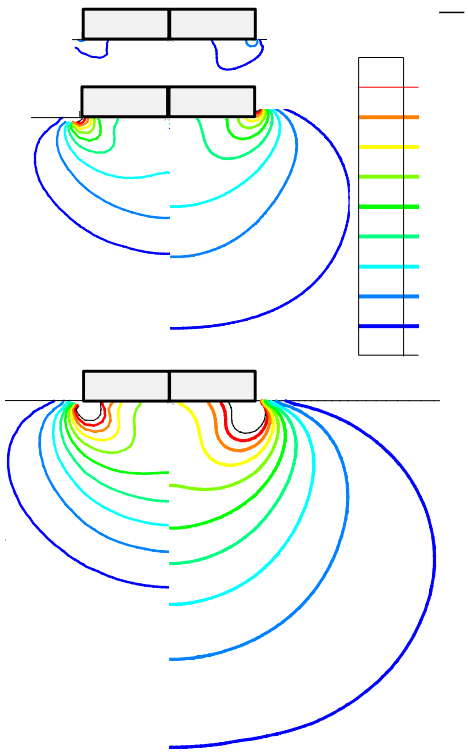

Figure 27. Contours of relative shear strength gain after full primary consolidation; circular and strip foundations.

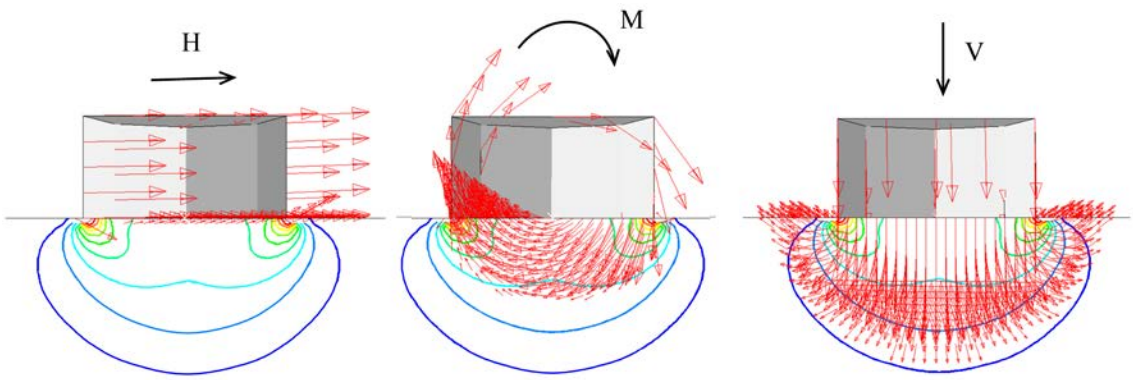

Figure 28. Failure mechanisms under pure horizontal, moment and vertical loading following preloading and consolidation for the discrete level of preload V_p/V_{uu} = 0.4 (circular foundation) (Contour lines represent the relative change in shear strength).

Published in *ASCE Journal of Geotechnical and Geoenvironmental Engineering*, 142(8), August http://dx.doi.org/10.1061/(ASCE)GT.1943-5606.0001498

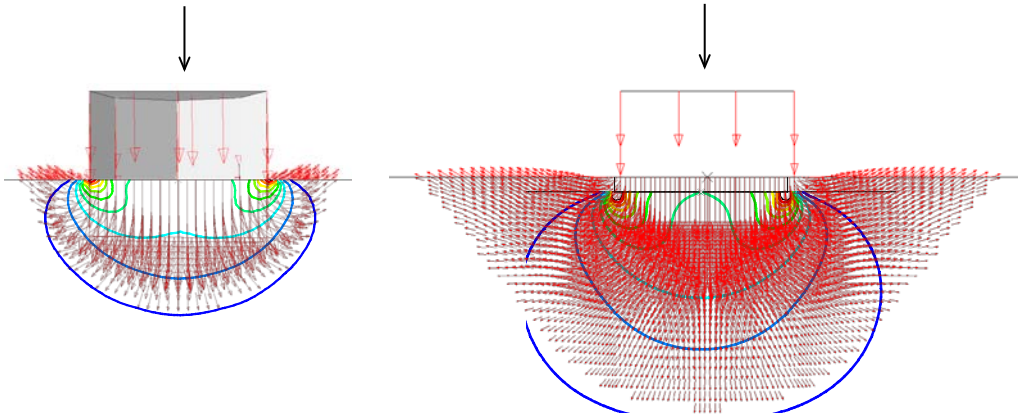

Figure 29. Comparison of failure mechanisms of circular and strip foundations under pure vertical loading following preloading and consolidation for a discrete level of preload V_p/V_{uu} = 0.4 (Contour lines represent the relative change in shear strength).

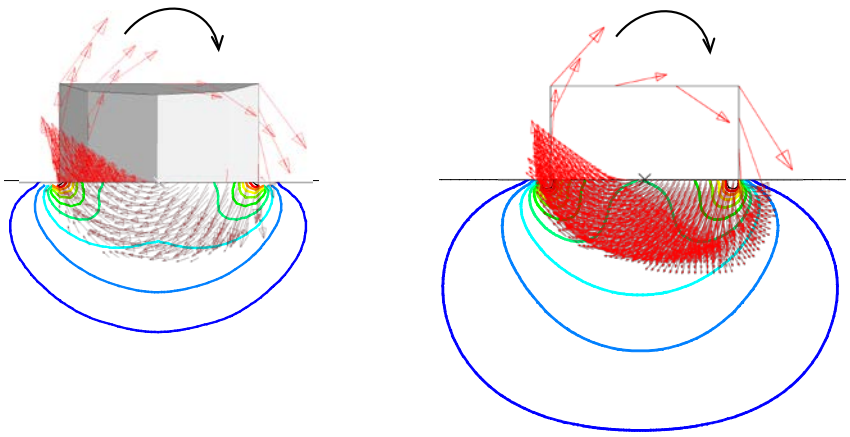

Figure 30. Comparison of failure mechanisms of circular and strip foundations under pure moment loading following preloading and consolidation for a discrete level of preload V_p/V_{uu} = 0.4 (Contour lines represent the relative change in shear strength).

Published in *ASCE Journal of Geotechnical and Geoenvironmental Engineering*, 142(8), August http://dx.doi.org/10.1061/(ASCE)GT.1943-5606.0001498

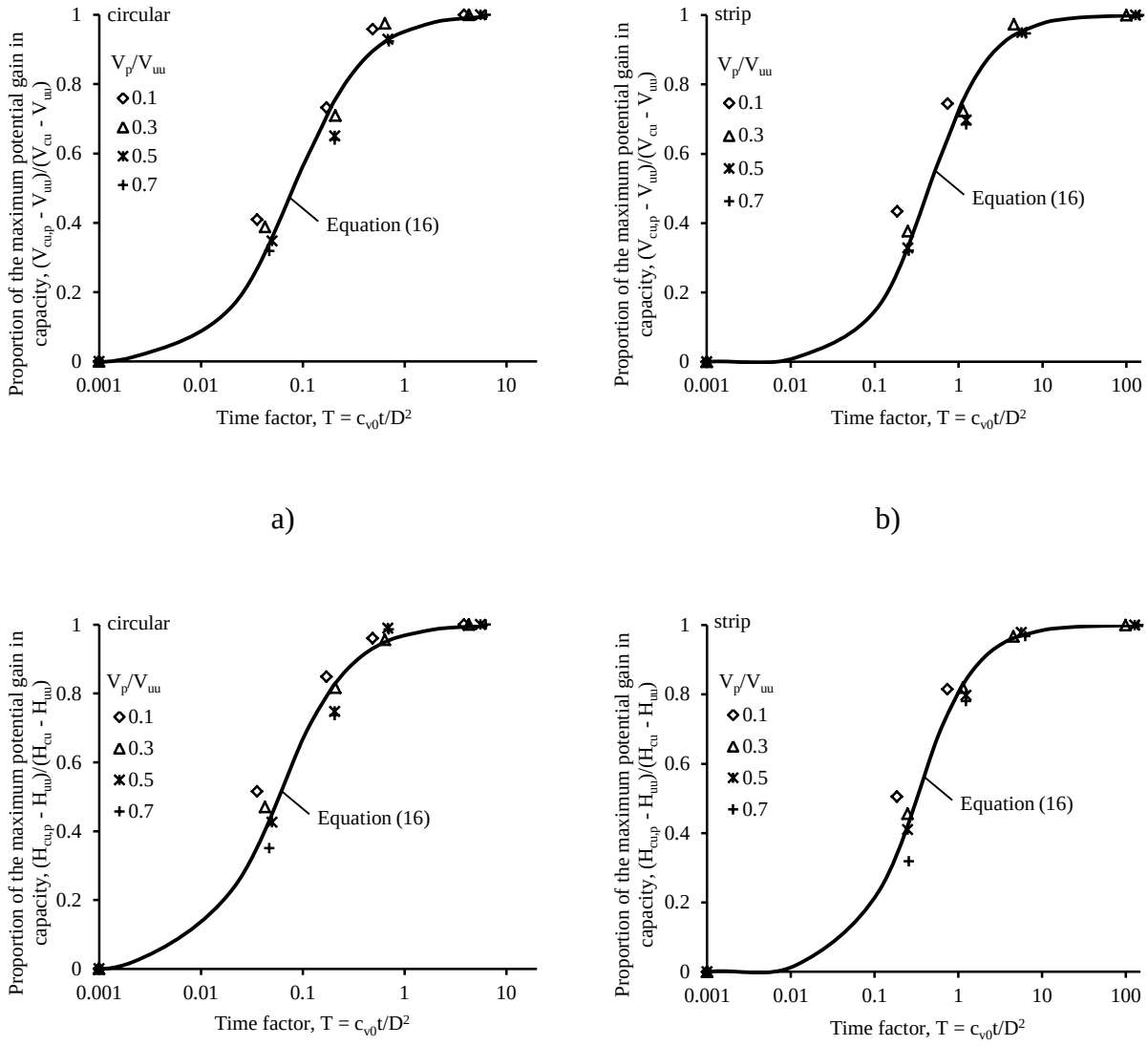

Figure 31. Gain in uniaxial capacity as a function of non-dimensional time factor T: comparison between FEA and Equation (16).

Published in *ASCE Journal of Geotechnical and Geoenvironmental Engineering*, 142(8), August http://dx.doi.org/10.1061/(ASCE)GT.1943-5606.0001498

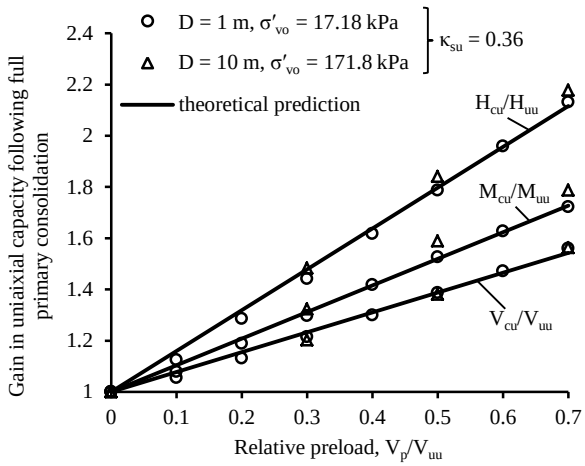

Figure 32. Sensitivity study showing applicability of theoretical framework to variations in foundation size of circular foundations for constant soil heterogeneity index κ_{su}.

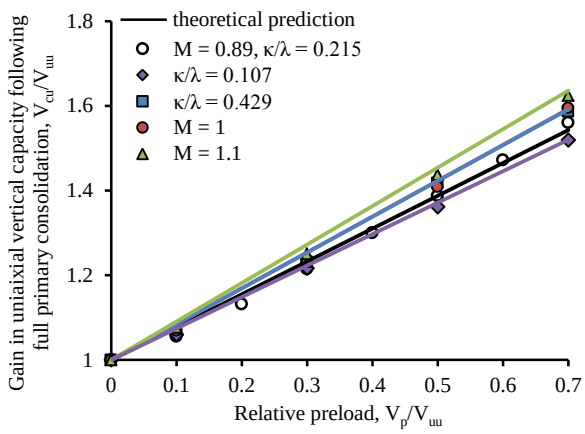

a) vertical

Published in *ASCE Journal of Geotechnical and Geoenvironmental Engineering*, 142(8), August http://dx.doi.org/10.1061/(ASCE)GT.1943-5606.0001498

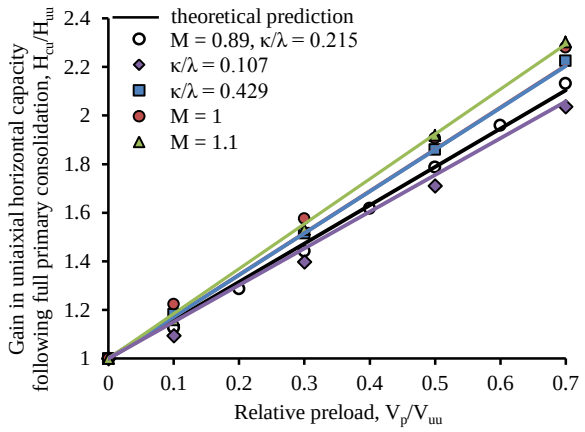

b) horizontal

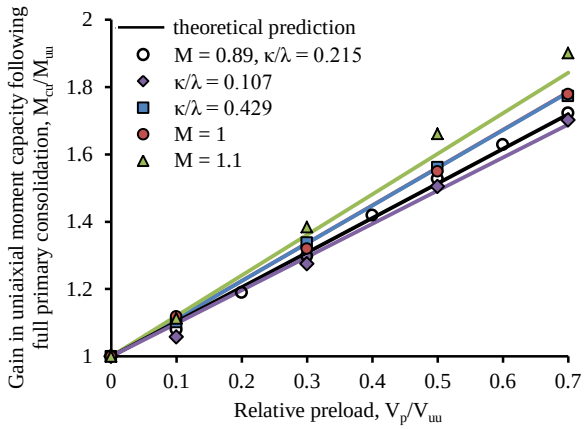

c) moment

Figure 33. Sensitivity study showing applicability of theoretical framework to varying MCC input for circular foundations

Published in *ASCE Journal of Geotechnical and Geoenvironmental Engineering*, 142(8), August http://dx.doi.org/10.1061/(ASCE)GT.1943-5606.0001498

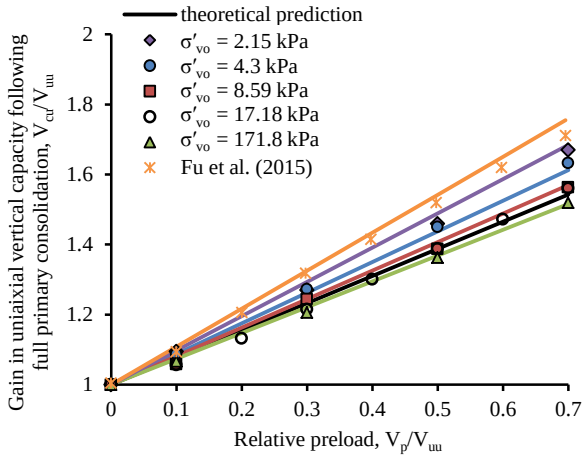

a) vertical

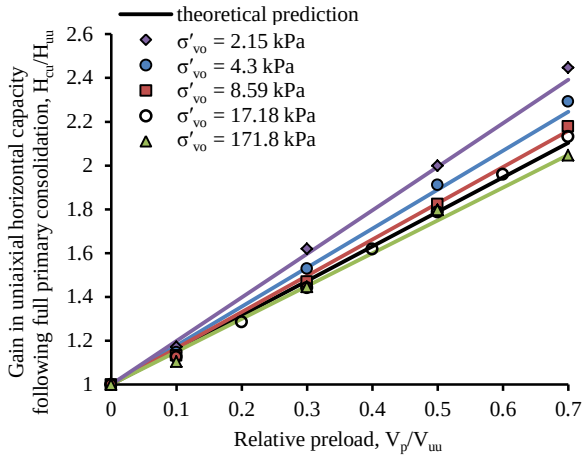

b) horizontal

Published in *ASCE Journal of Geotechnical and Geoenvironmental Engineering*, 142(8), August http://dx.doi.org/10.1061/(ASCE)GT.1943-5606.0001498

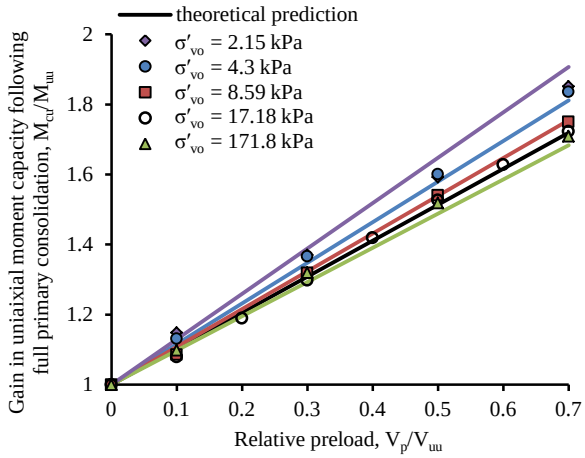

c) moment

Figure 34. Sensitivity study showing applicability of theoretical framework to varying overburden for constant foundation size for circular foundations.

Published in *ASCE Journal of Geotechnical and Geoenvironmental Engineering*, 142(8), August http://dx.doi.org/10.1061/(ASCE)GT.1943-5606.0001498

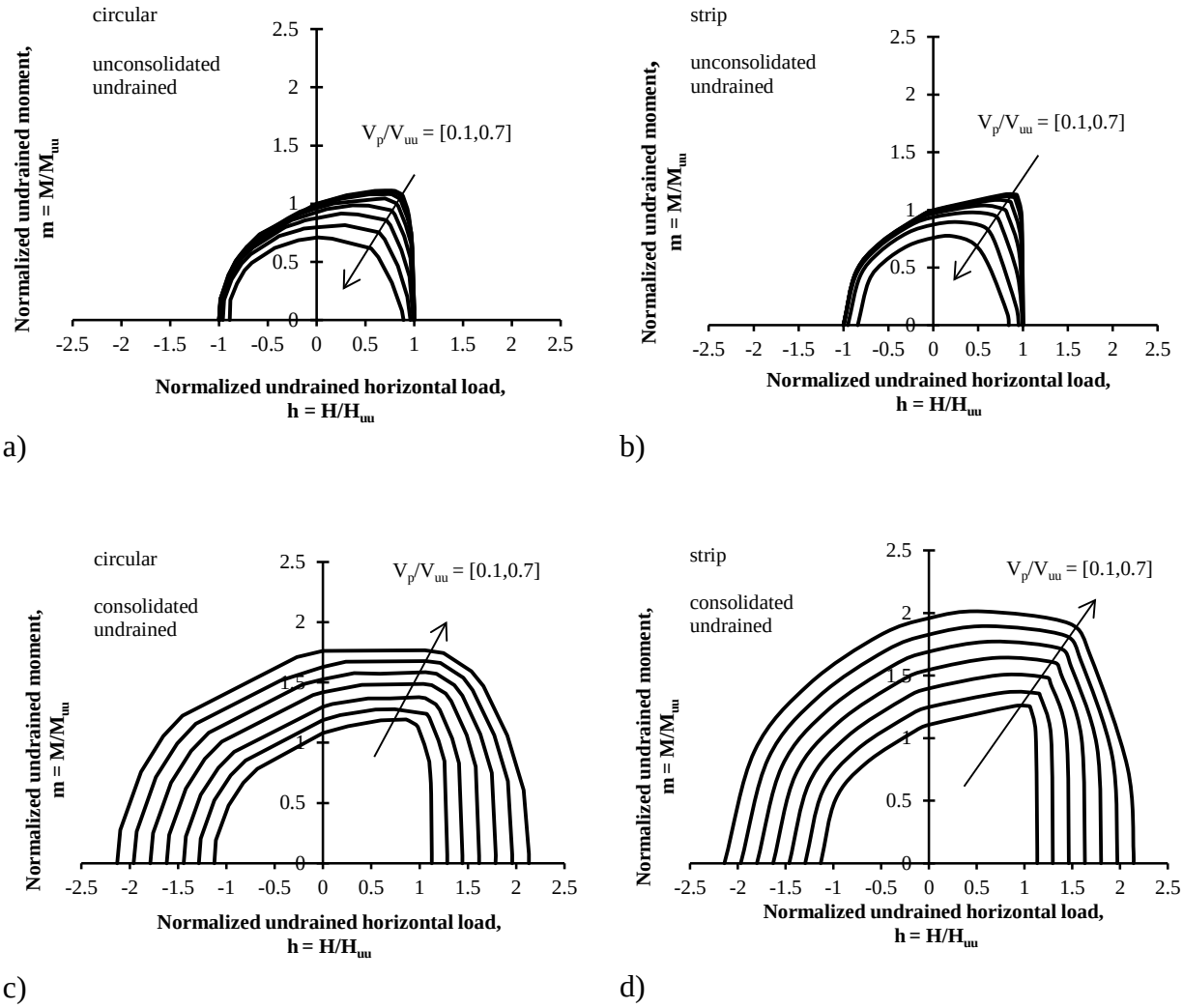

Figure 35. (a, b) Unconsolidated and (c, d) consolidated undrained failure envelopes as a function of relative preload for full primary consolidation (T_{99})

Published in *ASCE Journal of Geotechnical and Geoenvironmental Engineering*, 142(8), August http://dx.doi.org/10.1061/(ASCE)GT.1943-5606.0001498

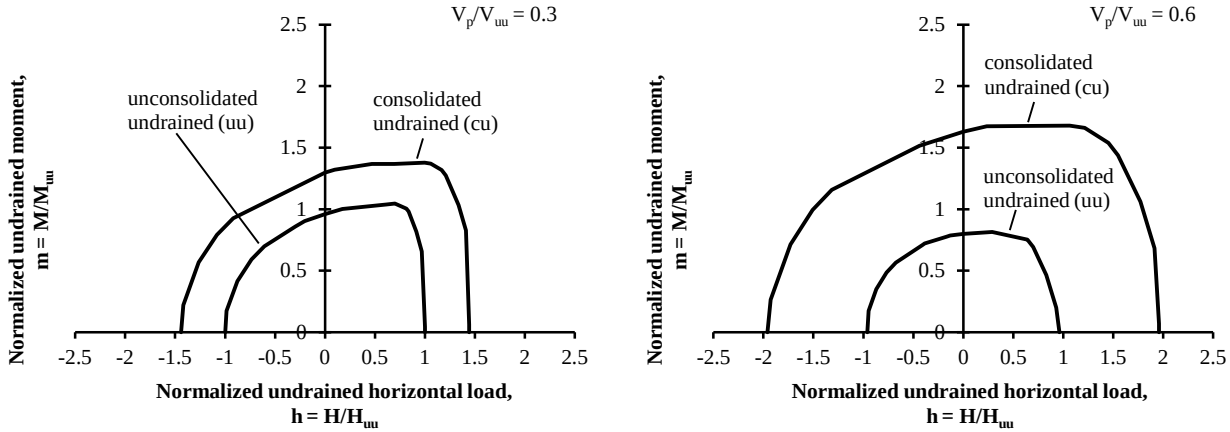

a) b)

Figure 36. Comparison of shape of normalized failure envelopes for unconsolidated and fully consolidated undrained capacity of a circular foundation: a) V_p/V_{uu} = 0.3, b) V_p/V_{uu} = 0.6.

Published in *ASCE Journal of Geotechnical and Geoenvironmental Engineering*, 142(8), August http://dx.doi.org/10.1061/(ASCE)GT.1943-5606.0001498

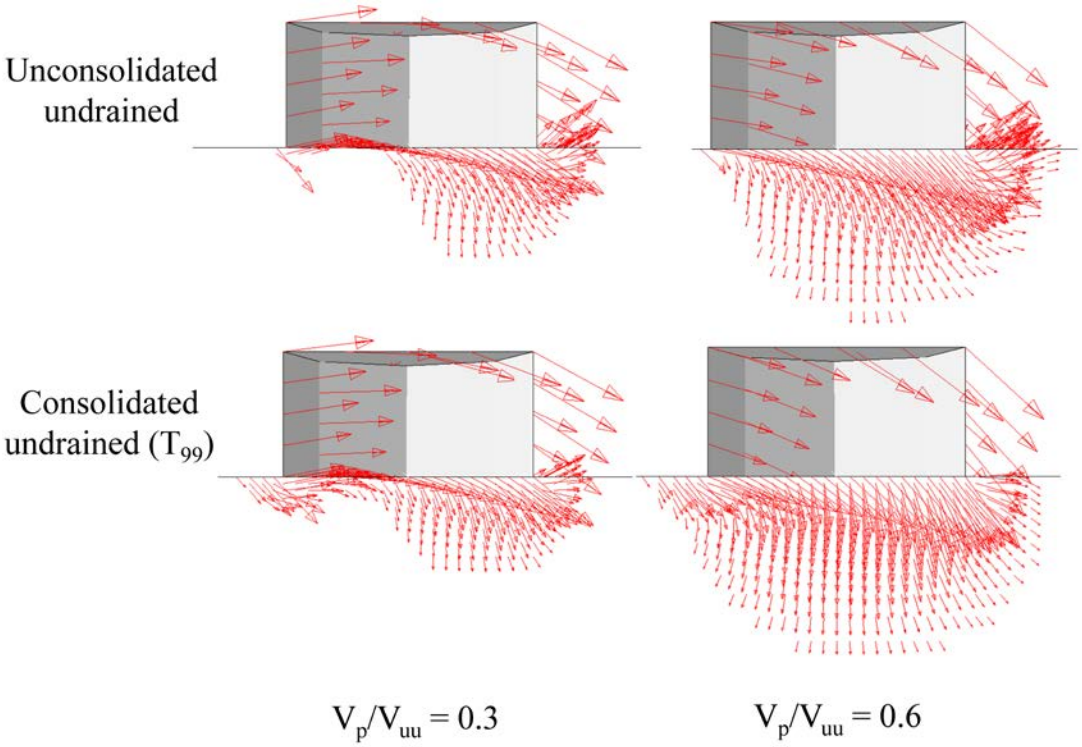

Figure 37. Failure mechanisms under undrained load paths to failure in HM space (u/Dθ = 1) for circular foundation.

Published in *ASCE Journal of Geotechnical and Geoenvironmental Engineering*, 142(8), August http://dx.doi.org/10.1061/(ASCE)GT.1943-5606.0001498

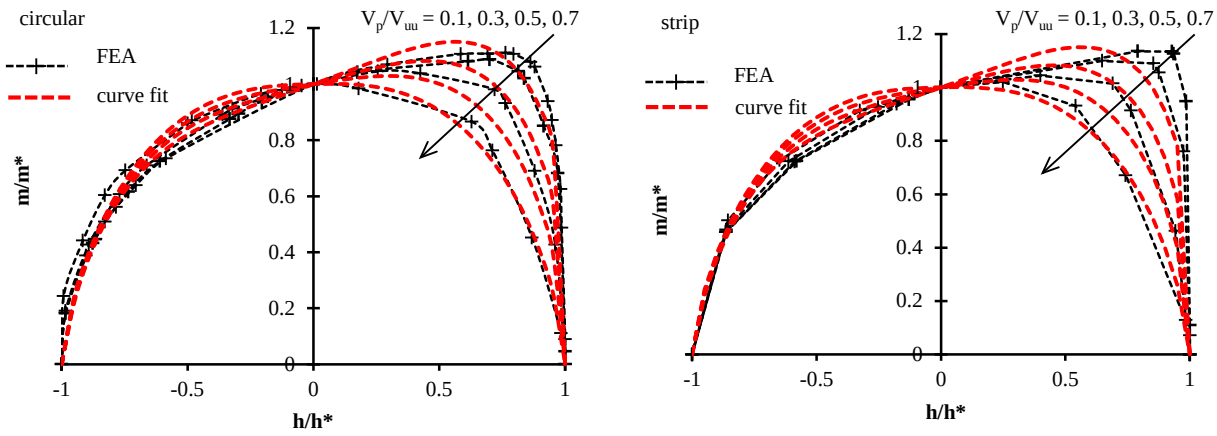

a) b)

Figure 38. Unconsolidated undrained normalized failure envelope for varying relative preload; FEA results and approximating expression (a) circular foundation and (b) strip foundation.

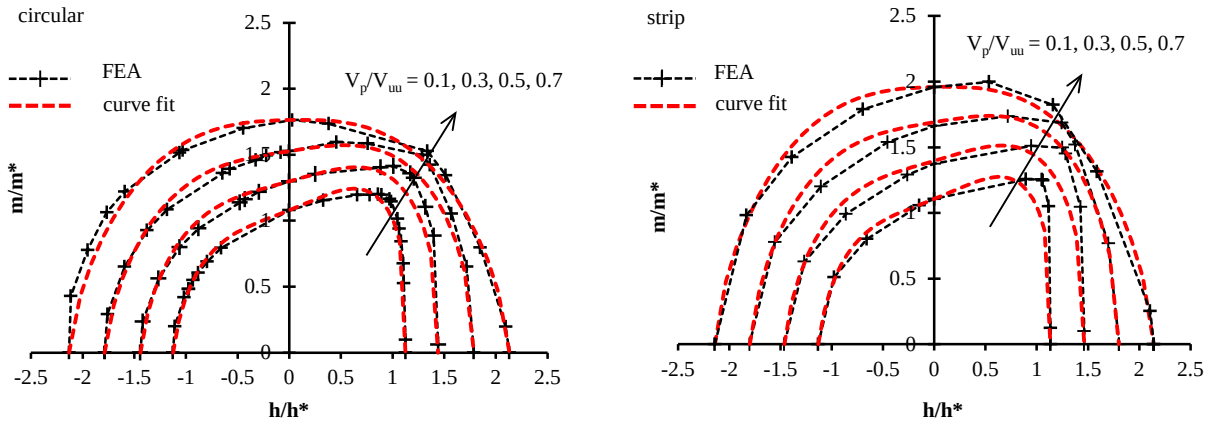

a) b)

Figure 39. Consolidated undrained normalized failure envelope for varying relative preload after full primary consolidation; FEA results and approximating expression (a) circular foundation and (b) strip foundation.

Published in *ASCE Journal of Geotechnical and Geoenvironmental Engineering*, 142(8), August http://dx.doi.org/10.1061/(ASCE)GT.1943-5606.0001498

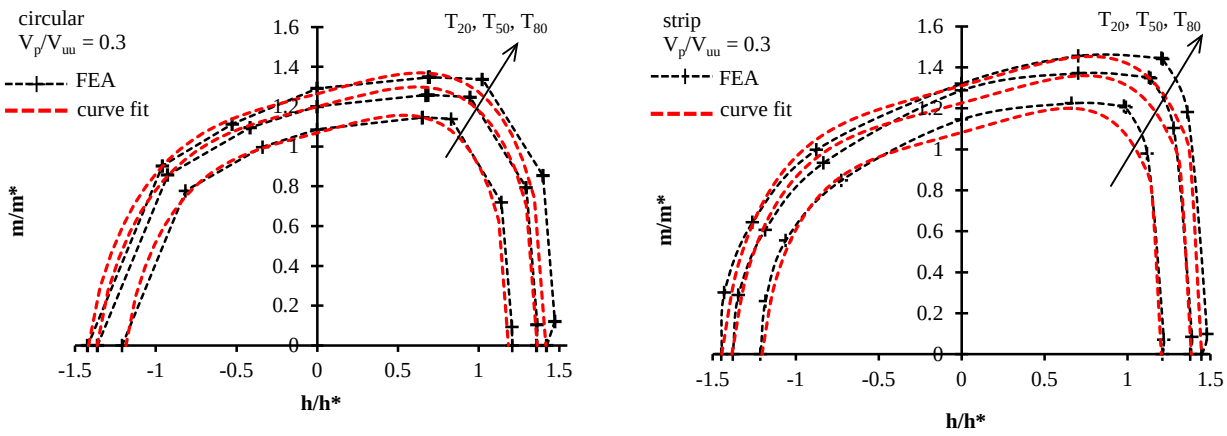

a) b)

Figure 40. Consolidated undrained normalized failure envelope for a discrete relative preload V_p/V_{uu} = 0.3 and varying consolidation times; FEA results and approximating expression (a) circular foundation and (b) strip foundation.